LETTER

doi:10.1038/nature11978

# Embryology of Early Jurassic dinosaur from China with evidence of preserved organic remains

Robert R. Reisz[1], Timothy D. Huang[2], Eric M. Roberts[3], ShinRung Peng[4], Corwin Sullivan[5], Koen Stein[6], Aaron R. H. LeBlanc[1], DarBin Shieh[4], RongSeng Chang[7], ChengCheng Chiang[8], Chuanwei Yang[9] & Shiming Zhong[10]

**Fossil dinosaur embryos are surprisingly rare, being almost entirely restricted to Upper Cretaceous strata that record the late stages of non-avian dinosaur evolution[1,2]. Notable exceptions are the oldest known embryos from the Early Jurassic South African sauropodomorph *Massospondylus*[3,4] and Late Jurassic embryos of a theropod from Portugal[5]. The fact that dinosaur embryos are rare and typically enclosed in eggshells limits their availability for tissue and cellular level investigations of development. Consequently, little is known about growth patterns in dinosaur embryos, even though post-hatching ontogeny has been studied in several taxa[6]. Here we report the discovery of an embryonic dinosaur bone bed from the Lower Jurassic of China, the oldest such occurrence in the fossil record. The embryos are similar in geological age to those of *Massospondylus* and are also assignable to a sauropodomorph dinosaur, probably *Lufengosaurus*[7]. The preservation of numerous disarticulated skeletal elements and eggshells in this monotaxic bone bed, representing different stages of incubation and therefore derived from different nests, provides opportunities for new investigations of dinosaur embryology in a clade noted for gigantism. For example, comparisons among embryonic femora of different sizes and developmental stages reveal a consistently rapid rate of growth throughout development, possibly indicating that short incubation times were characteristic of sauropodomorphs. In addition, asymmetric radial growth of the femoral shaft and rapid expansion of the fourth trochanter suggest that embryonic muscle activation played an important role in the pre-hatching ontogeny of these dinosaurs. This discovery also provides the oldest evidence of *in situ* preservation of complex organic remains in a terrestrial vertebrate.**

Monotaxic bone beds are prized by palaeobiologists because they yield large numbers of bones that can reveal patterns of development and growth within a single species[8]. Here we report the discovery of a monotaxic embryonic dinosaur bone bed in Lower Jurassic strata near Dawa, Lufeng County, Yunnan Province, China (specimens housed in the Chuxiong Prefectural Museum, catalogue no. C2019 2A233). The bone bed is equivalent in age to the oldest known dinosaurian embryos, preserved in South Africa[3]. The Chinese sauropodomorph bone bed is an accumulation of disarticulated skeletal elements representing various stages of embryonic development, rather than a set of articulated skeletons enclosed in eggs[9].

The bone bed was discovered in the Dark Red Beds or Zhangjia'ao member[10,11] of the Early Jurassic (Sinemurian, 190–197 Myr ago), Lower Lufeng Formation, roughly 3–5 m below the top of the Formation (Fig. 1). This unit is comparable temporally, environmentally and in faunal content to the Upper Elliot Formation of southern Africa[12] (Supplementary Information section 1), and preserves abundant skeletal remains of basal sauropodomorphs[13,14]. Taphonomically, the

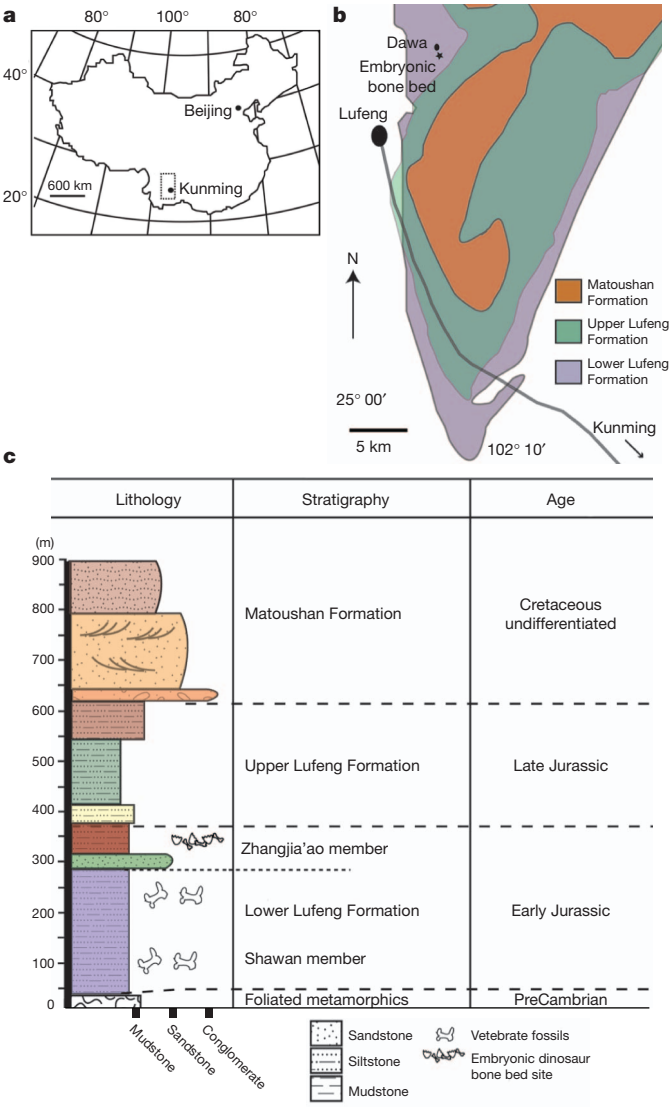


**Figure 1 | Location and stratigraphy of Lufeng monotaxic embryonic bone bed. a**, Map of China with study area in Yunnan Province shown by inset box. **b**, General geological map of the study area. **c**, Stratigraphic section showing location of the embryonic bone bed within Zhangjia'ao member of Lower Lufeng Formation.

[1]Department of Biology, University of Toronto Mississauga, Mississauga, Ontario L5L 1C6, Canada. [2]National Chung Hsing University, Taichung 402, Taiwan. [3]School of Earth and Environmental Sciences, James Cook University, Townsville, Queensland 4811, Australia. [4]Medical College Institute of Oral Medicine, National Cheng Kung University, Tainan 701, Taiwan. [5]Key Laboratory of Evolutionary Systematics of Vertebrates, Institute of Vertebrate Paleontology and Paleoanthropology, 100044 Beijing, China. [6]Steinmann Institüt für Geologie, Mineralogie und Paläontologie, University of Bonn, 53115 Bonn, Germany. [7]Department of Optics and Photonics, National Central University, Chung-Li 32001, Taiwan. [8]National Synchrotron Radiation Research Center, Hsinchu 30076, Taiwan. [9]Lufeng County Dinosaur Museum, Lufeng, Yunnan, China. [10]Chuxiong Prefectural Museum, 675000 Chuxiong, Yunnan, China.

10–20-cm-thick bone bed is characterized by the presence of completely disarticulated skeletal elements at various stages of embryonic development (Fig. 2), with calcium carbonate nodules often surrounding tightly packed appendicular skeletal elements. One nodule contains a high concentration of eggshell fragments that were apparently derived from soil compaction of a single egg, making it possible to obtain microstructural information about the oldest known terrestrial vertebrate eggshell (Supplementary Information section 2 and Supplementary Figs 2.1 and 2.2).

We interpret the bone bed as a para-autochthonous assemblage, formed by low-energy flooding and slow inundation of a colonial nesting site. The host sediment is a heavily bioturbated, massive siltstone, throughout which are dispersed isolated skeletal elements, eggshell fragments and the small, fossil-rich nodules of calcium carbonate.

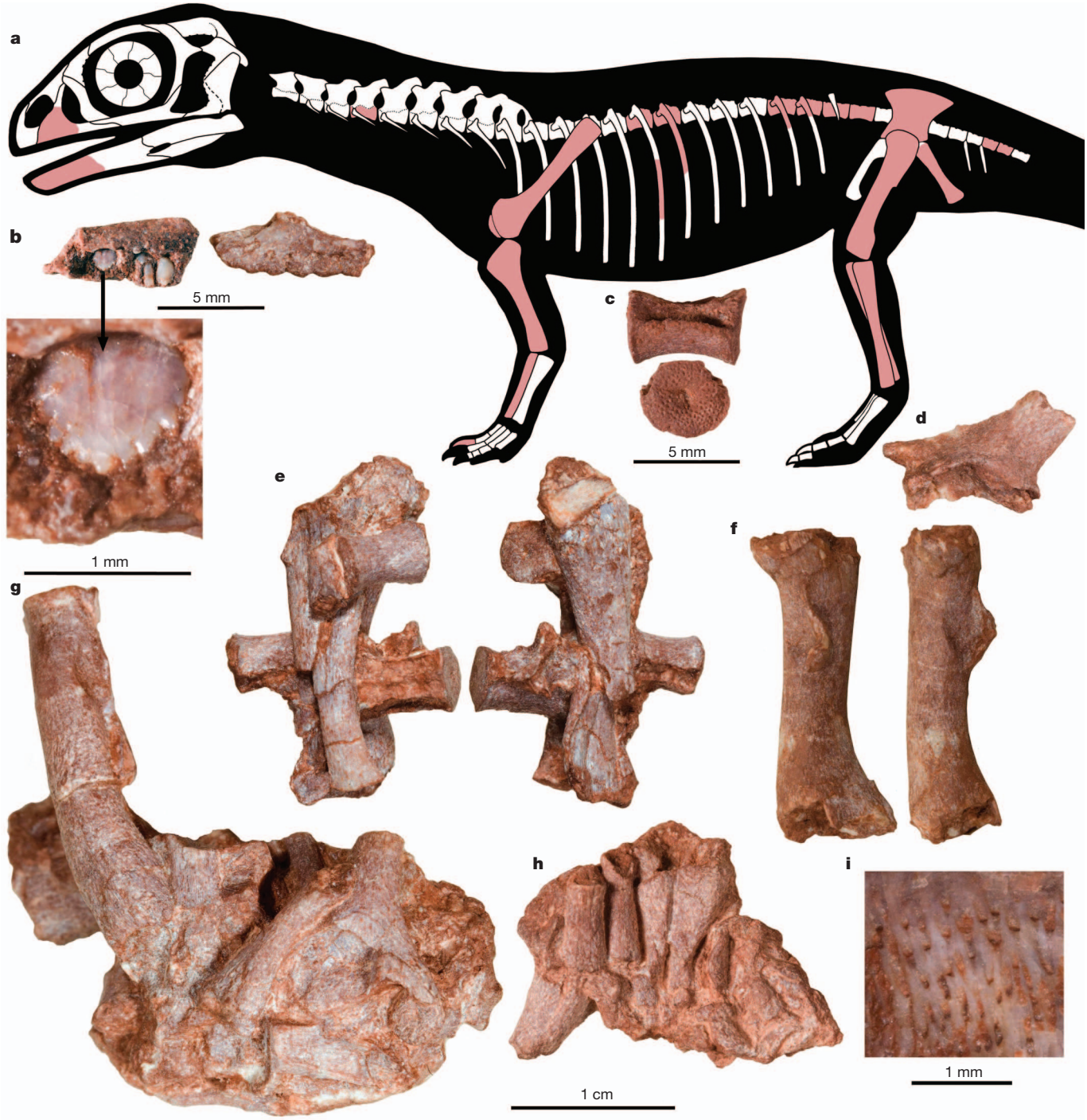


**Figure 2 | Sauropodomorph dinosaur embryonic skeletal elements from the Lufeng bone bed.** **a**, Reconstructed embryonic skeleton of Early Jurassic sauropodomorph (using *Massospondylus* as a model, not to scale), showing in dark red the known elements from Dawa (Chuxiong Prefectural Museum, no. C2019 2A233). Exact skeletal positions of numerous centra, ribs and distal limb elements are difficult to determine. **b**, Left maxillae in ventromedial and labial views, respectively, with enlarged view of partially erupted tooth. **c**, Mid-dorsal centrum in lateral and anterior views. **d**, Left ilium in lateral view. **e**, Right scapula, vertebrae and left humerus preserved in one nodule. **f**, Right femur in posterolateral and medial views, showing prominence and shape of the fourth trochanter. **g**, Large right femur preserved with ribs and various other skeletal elements in nodule. **h**, Embryonic limb elements and ribs showing alignment along long axes. **i**, Close-up of proximal end of right tibia, showing external foramina of primary cavities (vascular canals). Scale bar, 1 cm, unless otherwise shown.

There are no preserved nest structures or uncrushed eggs. The lack of coarse-grained sediment, coupled with the apparent sorting and concentration of bones (Fig. 2c, f, g) that are at various developmental stages, and hence from different nests, indicates that the bone bed is not an *in situ* nest or catastrophic death assemblage. We believe that inundation and ponding, followed by weak currents and simple wave action, explain the hydrodynamic sorting and non-random orientation of the disarticulated embryonic elements. Transport must have been minimal given the high preservational quality of the delicate, poorly ossified embryonic bones and <100-μm-thick eggshell. The embryonic bones and eggshell fragments were eventually buried and subjected to pedogenic processes, including precipitation of carbonate nodules that encase the bones.

The sample of more than 200 bones includes dozens of isolated cervical, dorsal, and caudal centra, rib fragments, femora and other limb elements, scapulae, an ilium, and a few skull elements (Fig. 2). These specimens are less ontogenetically advanced in multiple respects than some previously known sauropodomorph, theropod and ornithischian embryonic skeletons that were discovered inside intact eggs, demonstrating that the Lufeng specimens represent embryos rather than hatchlings[15]. Conspicuously embryonic features include the presence of teeth that do not protrude beyond the alveolar edges of the maxilla and dentary, centra with large notochordal canals and deeply pitted articular surfaces, and the universal presence of extensive primary vascular spaces that are open to the surface[16,17] (Supplementary Information section 3 and Supplementary Fig. 3).

The embryonic bones were compared with previously known saurischian and ornithischian embryos, and found to share detailed resemblances with embryos of other sauropodomorphs but not with those of ornithischians or theropods[1–3]. In particular, identification of the Lufeng specimens as sauropodomorphan was greatly facilitated by their similarity to the well known, articulated *Massospondylus* embryos[18]. Interpretation of the embryonic bones as representing a basal sauropodomorph is based on numerous features that are synapomorphies at various levels within basal Sauropodomorpha, and on a phylogenetic analysis using data from a recent study[19]. This analysis places the specimens well within the sauropodomorph clade but well outside Sauropoda, and supports their tentative referral to the well known Lufeng Formation sauropodomorph *Lufengosaurus*. Within Sauropodomorpha, the maxilla and its dentition show specific morphological resemblances to *Lufengosaurus*[7]. However, two other basal sauropodomorphs have also been recovered from the Lower Lufeng Formation of Yunnan[14], making identification of embryonic specimens as *Lufengosaurus* inescapably tentative (Supplementary Information section 4 and Supplementary Figs 4.1 and 4.2).

Histological study of the Lufeng embryonic specimens provides an unprecedented window into embryonic growth in a dinosaur because these fossils represent numerous individuals at various stages of embryonic development. For example, three thin-sectioned dorsal vertebrae show different stages in the embryonic development of the notochordal canal[16] (Fig. 3), a feature that is absent in individuals beyond the hatchling stage. Longitudinal sections of two vertebrae (Fig. 3a, b) show that the cranial and caudal ends consist mostly of hypertrophied calcified cartilage. The mid-regions of the vertebrae show an initial stage of highly cancellous bone deposition with numerous primary cavities ('vascular spaces'), indicative of very fast growth[20], and there is no evidence of any bone remodelling. A transverse section through the third vertebra (Fig. 3c) shows the notochordal canal as a large tunnel through the middle of the centrum, and reveals erosion cavities that indicate resorption of the cartilaginous precursor.

The sample includes 24 femora ranging from 2.6 to 4.5 mm in mid-shaft diameter, and 12 to 22 mm in length. They represent individuals from multiple nests[18], permitting the first morphometric analysis of embryonic growth in a dinosaur (Fig. 4a, Supplementary Information section 5 and Supplementary Figs 5.1–5.4). Thin sections through the mid-shaft regions and fourth trochanters of three femora of different

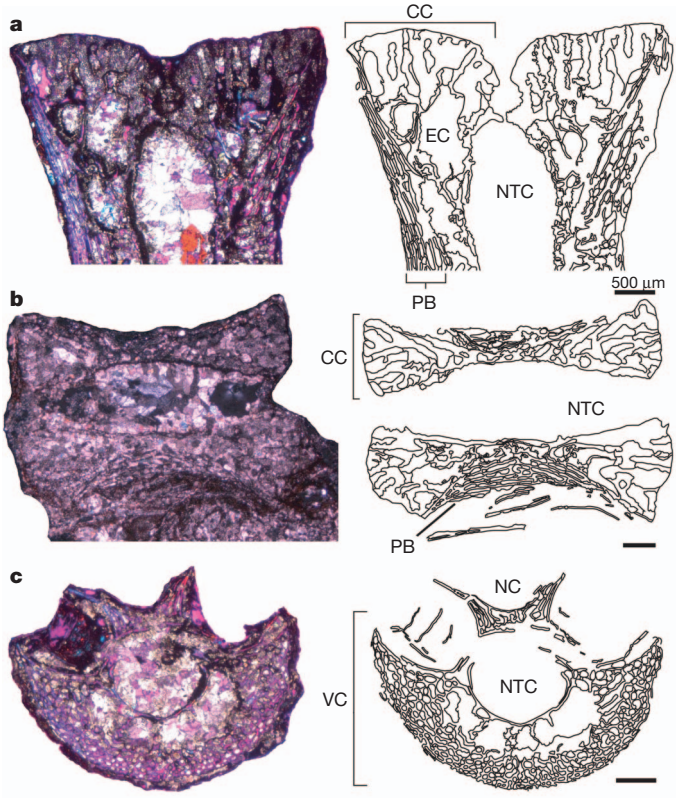


**Figure 3 | Embryonic vertebral histology (C2019 2A233).** **a**, Largest dorsal centrum, longitudinal section, cranial portion showing initial closure of notochordal canal and presence of erosion cavities with endochondral bone in the calcified cartilage. **b**, Smallest dorsal centrum, longitudinal section of whole bone, representing earlier embryonic stage with widely open notochordal canal. **c**, Intermediate-sized dorsal centrum, transverse section, showing notochordal canal. All scale bars represent 500 μm. Photographs taken with cross polar light with a lambda filter. CC, calcified cartilage; EC, erosion cavities; NC, neural canal; NTC, notochordal canal; PB, periosteal bone; and VC, vertebral centrum.

diameters also illustrate the development and ossification of the femur (Fig. 4b–d). The cross-sections show major differences in periosteal bone distribution, orientation of the vascular spaces (primary cavities), and size and level of ossification of the fourth trochanter (insertion site of the primary propulsive muscle of the hindlimb). In the smallest, least ossified femur (Fig. 4b), the fourth trochanter is small. In the mid-sized femur (Fig. 4c) the trochanter is more prominent, but contains little woven bone tissue. In the largest femur (Fig. 4d), the fourth trochanter is large and fully ossified. Mid-shaft cross-sections of seven femora, including the three already listed (Fig. 4b–d) show significantly greater vascularity (ratio of primary cavity area to total cross-sectional area of the cortex ranging from 56% to 65%) than in other dinosaurs, indicating a sustained very rapid rate of growth[20]. In addition, the femoral medullary cavity increases in diameter throughout embryonic development (Supplementary Fig. 5.4), indicating that, although the embryonic femur is composed entirely of primary bone, reshaping by endosteal bone resorption in the medullary cavity occurs even at this early ontogenetic stage. The high level of vascularity is the first known evidence that sauropodomorph embryos probably grew faster than those of extant birds and other dinosaurs, a circumstance that may imply that sauropodomorphs had shorter incubation times than their contemporaries. This capacity for rapid growth was evidently maintained after hatching[21], explaining the ability of sauropodomorphs to consistently achieve larger adult size than their dinosaurian contemporaries and in some cases reach gigantic proportions.

Extant vertebrates can display considerable limb and body movement before birth or hatching, involving muscle activation that mediates

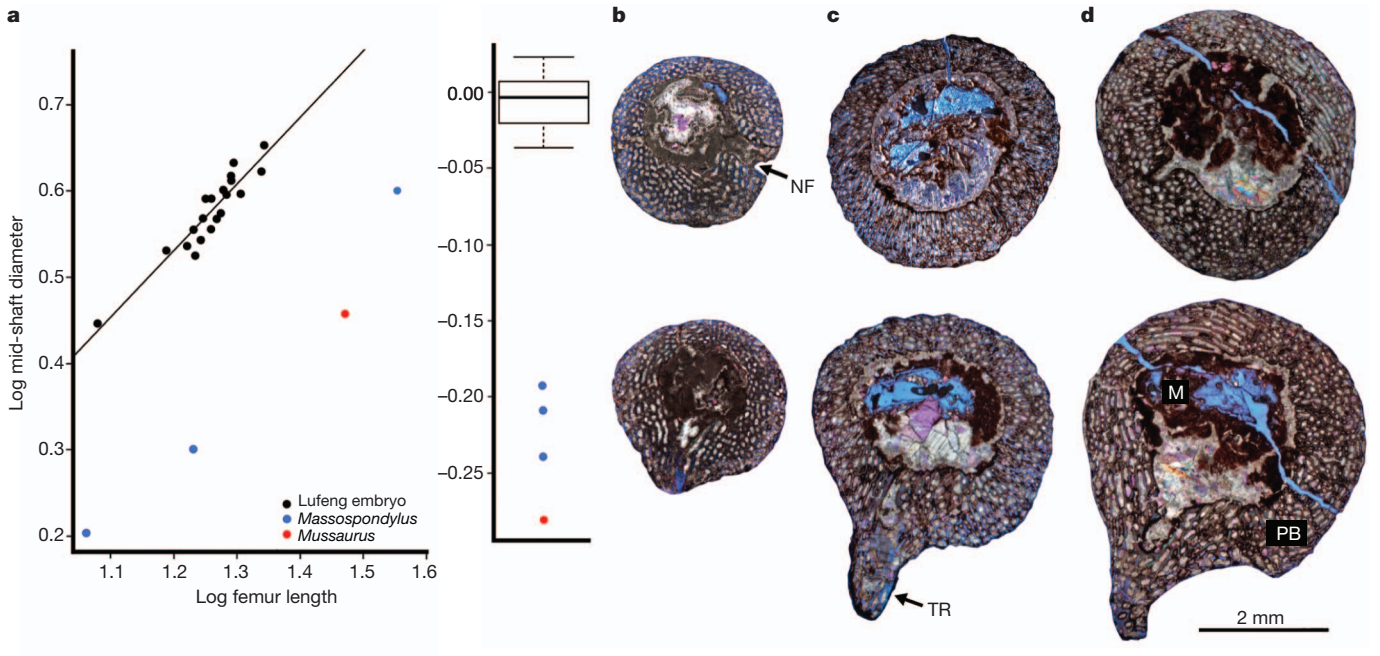


**Figure 4 | Embryonic femoral morphometric analysis and histology (C2019 2A233).** **a**, Results of regression analysis of Lufeng embryonic femora (black dots) showing growth trajectory of femoral mid-shaft diameter relative to length of femur, and box-plot of residuals. Lufeng femora show strong correlation between femoral length and shaft diameter ($R^2 = 0.8713$) and there are no outliers in this sample (see Supplementary Information section 5 and Supplementary Figs 5.1–5.4 for data and additional morphometric analyses). Two embryonic femora and one hatchling femur of the sauropodomorph *Massospondylus* (blue dots), and a hatchling femur of the sauropodomorph *Mussaurus* (red dot), are well outside the range of variation of the Lufeng embryos. **b–d**, Smallest to largest femora, sectioned transversely at mid-diaphysis above, and at the level of the fourth trochanter below. Photographs taken with cross polar light with a lambda filter. M, medullary cavity; NF, nutrient foramen; PB, primary periosteal bone with primary cavities ('vascular canals'); TR, fourth trochanter.

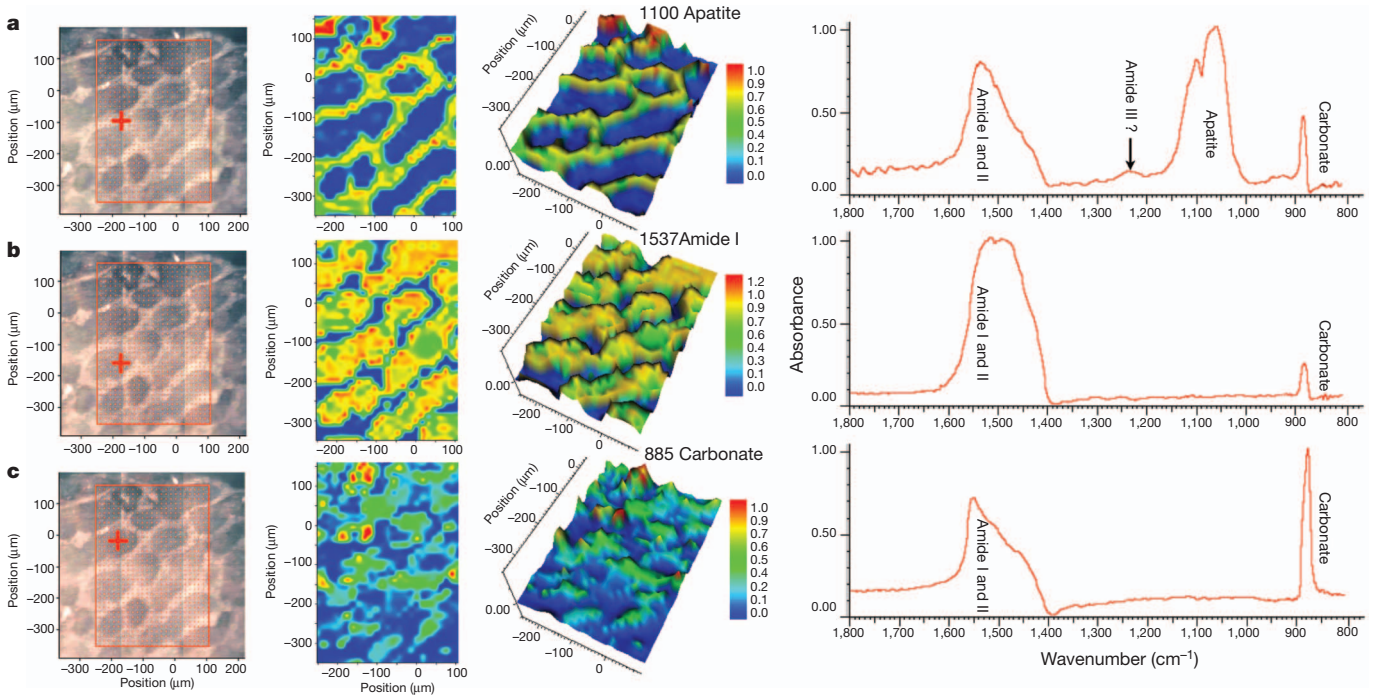


**Figure 5 | Synchrotron radiation Fourier transform infrared spectroscopy analysis of embryonic femur.** **a–c**, Different areas targeted within the bone. Images in each row include, from left to right: mosaic composed of 12 individual optical images (150 × 180 μm each), showing total Fourier transform infrared (FTIR) scanned area (red box), specific point targeted for analysis (red cross) and 15 μm step size (red dots); two-dimensional and three-dimensional FTIR distributions of absorption for the spectral band showing the highest intensity at the targeted point, with blue and red corresponding to low and high absorption, respectively; and Kramers–Kronig-transformed infrared spectrum for the targeted point. **a**, Primary bone tissue showing an apatite peak within primary bone but not within vascular spaces; primary bone tissue also shows an amide peak at 1,500–1,700 $cm^{-1}$, within apatite crystal. **b**, Edge of vascular space, near primary bone tissue, showing that margins of vascular spaces are characterized by the 1,537 $cm^{-1}$ amide peak but lack the apatite peak. **c**, Central area of a vascular canal, showing a 885 $cm^{-1}$ carbonate peak within vascular spaces; a modest amide peak at 1,537 $cm^{-1}$ is also present. We interpret the carbonate peak as the result of calcite infilling of the vascular canals.

skeletal development[22-24]. In mice and chickens this epigenetic phenomenon results in differential (asymmetrical) thickening of the walls of the long bones for improved load-bearing, resulting in geometry similar to that seen in the embryonic sauropodomorph femora. Similarly, sustained growth of skeletal crests and flanges depends on activation of the muscles attached to them, an observation that should be applicable to the dinosaurian fourth trochanter. It is probable that the uneven thickening of the femoral walls in the Lufeng specimens, the circumferential orientation of the primary vascular cavities, and the growth of the fourth trochanter (Fig. 4b–d) all depended upon muscle contraction and embryonic motility, an important mechanism for building a skeleton capable of coping with the functional demands encountered by the neonate. This discovery adds the first fossil evidence of such epigenetic phenomena to a growing body of research that documents their significance in extant model organisms.

The embryonic bones were also studied using synchrotron radiation-Fourier transform infrared (SR-FTIR) spectroscopy[25]. In contrast to previous studies of organic residues based on extracts obtained by decalcifying samples of bone, our approach targeted particular tissues *in situ* (Fig. 5). This made it possible to detect the preservation of organic residues, probably direct products of the decay of complex proteins, within both the fast-growing embryonic bone tissue and the margins of the vascular spaces (Fig. 5a, b). This is indicated by the multiple amide peaks revealed by both infrared (1,500–1,700 $cm^{-1}$ strong band from amide I and II, and 1,200–1,300 $cm^{-1}$ weak band from amide III) and Raman spectroscopy (amide A peak at 3,264 $cm^{-1}$) (Supplementary Figs 6.1 and 6.2). Previous reports of preserved dinosaur organic compounds, or 'dinosaurian soft tissues'[26–28], have been controversial because it was difficult to rule out bacterial biofilms or some other form of contamination as a possible source of the organics[29]. Our results clearly indicate the presence of both apatite and amide peaks within woven embryonic bone tissue (Fig. 5a), which should not be susceptible to microbial contamination or other post-mortem artefacts.

## METHODS SUMMARY

Fossil preparation was done manually under a dissecting microscope. Thin sections ranging from 30 to 50 μm in thickness were photographed using a Nikon AZ100 microscope with a lambda filter. Image J software was used to calculate the percentage vascularity (ratio between the total area of the primary cavities and the overall area of the cortex) of each femoral thin section. NIS Elements imaging software for the Nikon DS-Fi2 mounted digital camera was used both for photography and confirmation of percentage vascularity. For FTIR analysis, infrared spectral line scans and mapping data were collected using the SR-FTIR spectromicroscopy facility at the National Synchrotron Radiation Research Center (NSRRC) beamline 14A1 (BL14A1) in Taiwan. The spectra were recorded in reflectance mode from each sample section using a Thermo Nicolet 6700 FTIR spectrometer and continuum infrared microscope with the following settings: resolution 4 $cm^{-1}$, step size 15 μm, aperture size 30 μm and 128 scans. Peak position and baseline corrections were performed using OMNIC peak resolving software.

**Received 25 October 2012; accepted 4 February 2013.**


1. Carpenter, K., Hirsch, K. F. & Horner, J. R. (eds). *Dinosaur Eggs and Babies* (Cambridge Univ. Press, 1994).
2. Chiappe, L. M. *et al.* Sauropod dinosaur embryos from the Late Cretaceous of Patagonia. *Nature* **396,** 258–261 (1998).
3. Reisz, R. R., Scott, D., Sues, H.-D., Evans, D. C. & Raath, M. A. Embryos of an Early Jurassic prosauropod dinosaur and their evolutionary significance. *Science* **309,** 761–764 (2005).
4. Reisz, R. R., Evans, D. C., Roberts, E. M., Sues, H.-D. & Yates, A. M. Oldest known dinosaurian nesting site and reproductive biology of the Early Jurassic sauropodomorph *Massospondylus*. *Proc. Natl Acad. Sci. USA* **109,** 2428–2433 (2012).
5. de Ricqlès, A., Mateus, O., Antunes, M. T. & Taquet, P. Histomorphogenesis of embryos of Upper Jurassic theropods from Lourinhã (Portugal). *C. R. Acad. Sci. IIA* **332,** 647–656 (2001).
6. Padian, K., de Ricqlès, A. J. & Horner, J. R. Dinosaurian growth rates and bird origins. *Nature* **412,** 405–408 (2001).
7. Young, C. C. A complete osteology of *Lufengosaurus huenei* Young (gen. et sp. nov) from Lufeng, Yunnan, China. *Palaeontol. Sinica New Series C* **7,** 1–53 (1941).
8. Rogers, R. R., Eberth, D. A. & Fiorillo, A. R. (eds). *Bonebeds, Genesis, Analysis, and Paleobiological Significance* (Chicago Univ. Press, 2007).
9. Carpenter, K. *Eggs, Nests, and Baby Dinosaurs. A Look at Dinosaur Reproduction* (Indiana Univ. Press, 1999).
10. Bien, M. N. "Red Beds" of Yunnan. *Bull. Geol. Soc. China* **21,** 159–198 (1941).
11. Fang, X. *et al.* in *Proc. Third National Stratigraphical Congress of China.* 208–214 (Geological Publishing House, 2000).
12. Weishampel, D. B., Dodson, P. & Osmólska, H. (eds). *The Dinosauria* (Univ. California Press, 2004).
13. Sun, A. G. & Cui, K. H. in *The Beginning of the Age of Dinosaurs* (ed. Padian, K.) 275–278 (Cambridge Univ. Press, 1986).
14. Galton, P. M. & Upchurch, P. in *The Dinosauria* (eds Weishampel D. B., Dodson, P. & Osmólka, H.) 232–258 (Univ. California Press, 2004).
15. Kundrát, M., Cruickshank, A. R. I., Manning, T. W. & Nudds, J. Embryos of therizinosauroid theropods from the Upper Cretaceous of China: diagnosis and analysis of ossification patterns. *Acta Zool. (Stockh.)* **89,** 231–251 (2008).
16. Fleming, A., Keynes, R. J. & Tannahill, D. The role of the notochord in vertebral column formation. *J. Anat.* **199,** 177–180 (2001).
17. Francillon-Vieillot, H. *et al.* in *Skeletal Biomineralization: Patterns, Processes and Evolutionary Trends* (ed. Carter, J. G.) 471–530 (Van Nostrand Reinhold, 1990).
18. Reisz, R. R., Sues, H. D., Evans, D. C. & Scott, D. Embryonic skeletal anatomy of the saudopodomorph dinosaur *Massospondylus* from the Lower Jurassic of South Africa . *J. Vertebr. Palaeontol.* **30,** 1653–1665 (2010).
19. Apaldetti, C., Pol, D. & Yates, A. The postcranial anatomy of *Coloradisaurus brevis* (Dinosauria: Sauropodomorpha) from the Late Triassic of Argentina and its phylogenetic implications. *Palaeontology* http://dx.doi.org/10.1111/j.1475-4983.2012.01198.x (22 November 2012).
20. Horner, J. R., Padian, K. & Ricqlès, A. D. Comparative osteohistology of some embryonic and perinatal archosaurs: developmental and behavioural implications for dinosaurs. *Paleobiology* **27,** 39–58 (2001).
21. Sander, M. P. Longbone histology of the Tendaguru sauropods: implications for growth and biology. *Paleobiology* **26,** 466–488 (2000).
22. Müller, G. B. Embryonic motility: environmental influences and evolutionary innovation. *Evol. Dev.* **5,** 56–60 (2003).
23. Sharir, A., Stern, T., Rot, C., Shahar, R. & Zelzer, E. Muscle force regulates bone shaping for optimal load-bearing capacity during embryogenesis. *Development* **138,** 3247–3259 (2011).
24. Blitz, E. *et al.* Bone ridge patterning during musculoskeletal assembly is mediated through SCX regulation of *Bmp4* at the tendon-skeleton junction. *Dev. Cell* **17,** 861–873 (2009).
25. Kong, J. & Shaoning, Y. Fourier transform infrared spectroscopic analysis of protein secondary structures. *Acta Biochim. Biophys. Sin. (Shanghai)* **39,** 549–559 (2007).
26. Schweitzer, M. H., Wittmeyer, J. L., Horner, R. H. & Toporski, J. K. Soft-tissue vessels and cellular preservation in *Tyrannosaurus rex*. *Science* **307,** 1952–1955 (2005).
27. Schweitzer, M. H. *et al.* Analyses of soft tissue from *Tyrannosaurus rex* suggest the presence of protein. *Science* **316,** 277–280 (2007).
28. Lindgren, J. *et al.* Microspectroscopic evidence of Cretaceous bone proteins. *PLoS ONE* **6,** e19445 (2011).
29. Kaye, T. G., Gaugler, G. & Sawlowicz, Z. Dinosaurian soft tissue interpreted as bacterial biofilms. *PLoS ONE* **3,** e2808 (2008).


**Supplementary Information** is available in the online version of the paper.

**Acknowledgements** We thank D. Scott for specimen preparation, photography, and figure preparation; N. Campione for morphometric analysis; C. Apaldetti for the data matrix; O. Dülfer for thin sections; G. Grellet-Tinner, M. Sander, J. Steigler, P. Barrett and E. Prondvai for discussion; C. Chu and X. J. Lin for research support; S. P. Modesto and C. Brown for field assistance; J. Liu for assistance in Lufeng; and C. C. Wang, Y. F. Song, Y. C. Lee and H. S. Sheu for help with various experiments at the National Synchrotron Radiation Research Center, Taiwan. Research support was provided by NSERC Discovery and SRO Grants (Canada), University of Toronto, DFG FOR 533 (contribution 130) (Germany), NSC 100-2116-M-008-016 (Taiwan), Ministry of Education (Taiwan) under the NCKU Aim for the Top University Project, Chinese Academy of Sciences and National Natural Science Foundation of China (41150110341).

**Author Contributions** R.R.R. jointly conceived and designed the project with T.D.H.; R.R.R. wrote the paper, and supervised preparation and scientific illustration of specimens; T.D.H., E.M.R., C.S., K.S. and A.R.H.L., contributed to the manuscript; R.R.R., T.D.H., E.M.R., C.S., R.C. and C.Y. contributed to field work; T.D.H., S.P. and D.S. supervised and completed multimodal optical and chemical spectroscopic analyses; K.S., A.R.H.L. and C.C. prepared slides and illustrated thin sections; R.R.R., T.D.H., K.S., E.M.R., S.P. and C.S. wrote the Supplementary Information; T.D.H., R.C., C.Y. and S.Z. provided logistical support for field work and research.

**Author Information** Reprints and permissions information is available at www.nature.com/reprints. The authors declare no competing financial interests. Readers are welcome to comment on the online version of the paper. Correspondence and requests for materials should be addressed to R.R.R. (robert.reisz@utoronto.ca).